# Supporting Information

## Fe-functionalised N-doped $Ti_3C_2T_z$ MXene for the alkaline oxygen reduction reaction

Luc Bouscarrat[a,b], Alex Scrimshire[c], Paul A. Bingham[c], Gaurav Gupta[a], Richard Dawson[a,d] and Nuno Bimbo[a,e]

[a] *School of Engineering, Gillow Avenue, Lancaster University, LA1 4YW, UK*

[b] *AFC Energy PLC, Dunsfold Park, Canada Avenue, Cranleigh, GU6 8TB, UK*

[c] *School of Engineering and Built Environment, Sheffield Hallam University, City Campus Howard Street, Sheffield, S1 1WB, U.K.*

[d] *LiNa Energy, White Cross Industrial Estate, South Rd, Lancaster, LA1 4XQ, UK*

[d] *School of Chemistry and Chemical Engineering, Highfield Campus, University of Southampton, Southampton, SO17 1BJ, UK*

### Powder X-ray diffraction

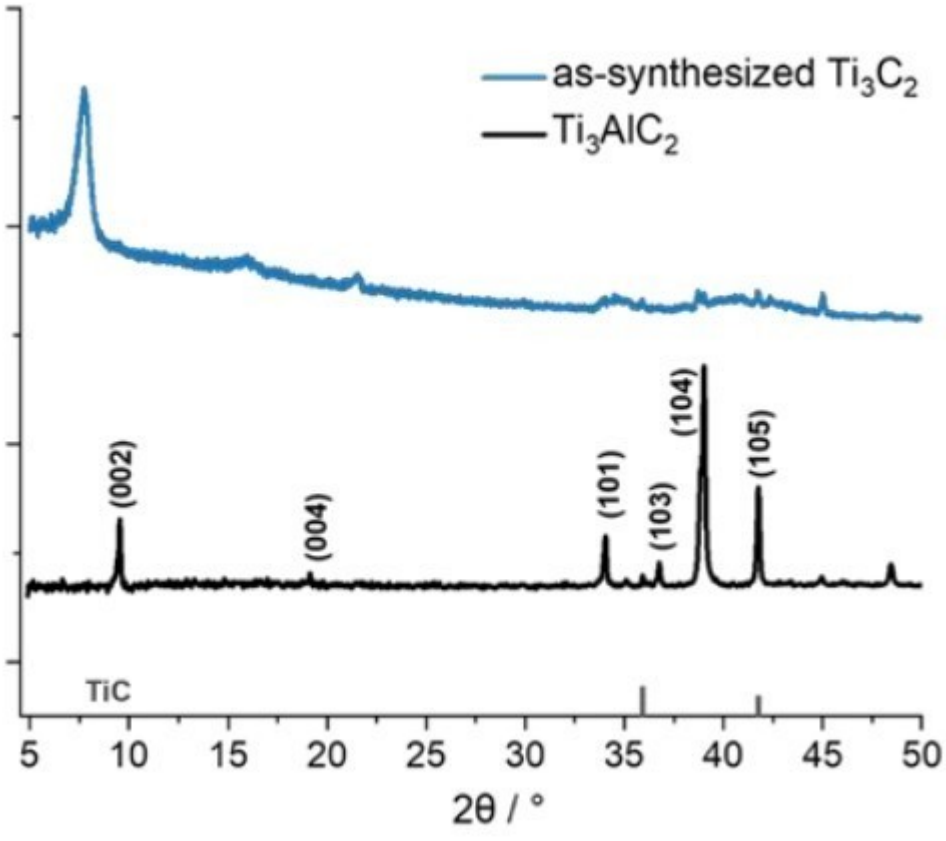


**Figure S1** Powder X-ray diffraction pattern for the precursor MAX phase ($Ti_3AlC_2$) and the as-synthesised MXene ($Ti_3C_2T_z$).

## EDS

Elemental analysis of samples $Ti_3C_2$-U10-Fe-800 and $Ti_3C_2$-U50-Fe-800 was performed using Energy Dispersive X-ray Spectroscopy (EDS). The EDS mapping is shown in Figure S2 and the elemental composition is presented in Table S1.

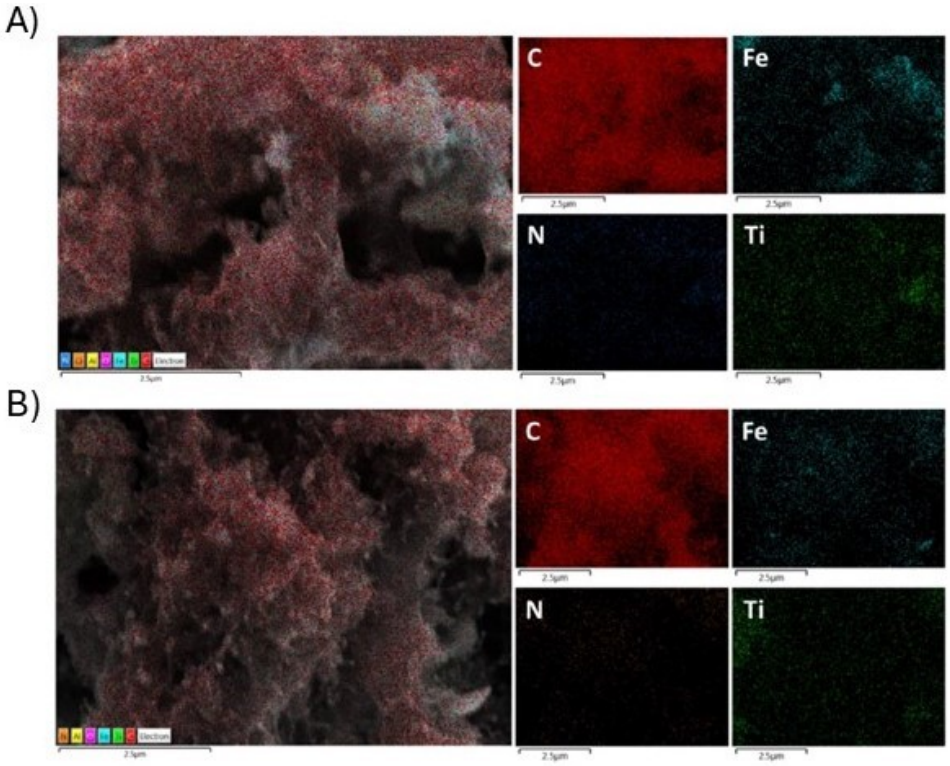


**Figure S2** Elemental composition obtained from EDS for A) $Ti_3C_2$-U10-Fe-800 and B) $Ti_3C_2$-U50-Fe-800. Right-hand side are the elements C, Fe, N and Ti and left-hand side is the superimposed picture of all these elements.

The urea decomposition products react with the supporting materials during the thermal treatment to form nitrogen and carbon compounds. This agrees with the XRD results presented in the manuscript, where a small graphitic carbon peak appears in both samples. The carbon, nitrogen and iron ratios are determined for comparison between samples, with the atomic proportions of Ti and Fe similar for both $Ti_3C_2$-U10-Fe-800 and $Ti_3C_2$-U50-Fe-800, as the amount of $Ti_3C_2$ and $FeCl_3$ used in the synthesis was the same for both samples. It can be seen in Figure S2 that carbon is highly distributed in the samples, indicating that carbon species have covered most of the MXene flakes. The N signal also shows a relatively homogeneous distribution in the samples, while the Fe map shows even Fe distribution for the $Ti_3C_2$-U50-Fe-800 while the Fe seems less homogeneous and more aggregated in specific regions in the $Ti_3C_2$-U10-Fe-800.

**Table S1** EDS elemental composition of $Ti_3C_2$-Ux-Fe-800 samples averaged over three measurements.

| (at. %) | Ti | C (C/Ti ratio) | O | N (N/Ti ratio) | Fe (Fe/Ti) | Cl | Al |
|---|---|---|---|---|---|---|---|
| $Ti_3C_2$-U10-Fe-800 | 11.3 ± 3.9 | 70.1 ± 6.2 (6.20) | 9.8 ± 0.2 | 3.6 ± 1.5 (0.32) | 4.2 ± 0.4 (0.37) | 0.8 ± 0.2 | 0.2 ± 0.1 |
| $Ti_3C_2$-U50-Fe-800 | 10.7 ± 1.3 | 63.8 ± 6.5 (5.96) | 13.5 ± 3.8 | 6.5 ± 2.3 (0.61) | 4.4 ± 1.2 (0.41) | 0.3 ± 0.2 | 0.4 ± 0.3 |

## $^{57}$Fe Mössbauer spectroscopy

The Fe-species assignment of the deconvolution of the spectra is based on the literature [1-3]. The site parameters and composition of the samples are presented in Tables S2, S3 and S4.

**Table S2** $^{57}$Fe Mössbauer spectroscopy fitted site parameters and composition for the $Ti_3C_2$-U50-800 sample.

| | CS (mm/s) | Δ (mm/s) | A (counts.mm/s) | $w_+$ (mm/s) | $A_-/A_+$ | $w_-/w_+$ | Composition |
|---|---|---|---|---|---|---|---|
| Doublet 1 | 0.409 (81) | 0.91 (14) | 4590 (820) | 0.38 (12) | 1* | 1* | 18.3 (33) |
| | **CS (mm/s)** | **ε (mm/s)** | **A (counts.mm/s)** | **H(T) (mm/s)** | **$w_3$ (mm/s)** | | **Composition** |
| Sextet 1 | -0.034 (46) | 0.034 (45) | 6000 (1300) | 32.84 (26) | 0.207 (57) | | 23.8 (53) |
| Sextet 2 | 0.192 (15) | 0.010 (15) | 14500 (1200) | 20.80 (11) | 0.192 (20) | | 57.9 (48) |
| **Reduced $\chi^2$ = 0.543452** | | | | | | | |

**Table S3** $^{57}$Fe Mössbauer spectroscopy fitted site parameters and composition for the $Ti_3C_2$-U10-800 sample.

| | CS (mm/s) | Δ (mm/s) | A (counts.mm/s) | $w_+$ (mm/s) | $A_-/A_+$ | $w_-/w_+$ | Composition |
|---|---|---|---|---|---|---|---|
| Doublet 1 | 0.315 (31) | 0.916 (52) | 5450 (470) | 0.291 (41) | 1* | 1* | 15.8 (14) |
| | **CS (mm/s)** | **ε (mm/s)** | **A (counts.mm/s)** | **H(T) (mm/s)** | **$w_3$ (mm/s)** | | **Composition** |
| Sextet 1 | 0.002 (21) | 0.023 (21) | 5440 (740) | 33.43 (12) | 0.155 (27) | | 15.8 (21) |
| Sextet 2 | 0.1922 (63) | 0.0070 (63) | 23520 (770) | 20.313 (47) | 0.1989 (85) | | 68.3 (22) |
| **Reduced $\chi^2$ = 0.831822** | | | | | | | |

**Table S4** $^{57}$Fe Mössbauer spectroscopy fitted site parameters and composition for the C-U50-800 sample.

| | CS (mm/s) | Δ (mm/s) | A (counts.mm/s) | $w_+$ (mm/s) | $A_-/A_+$ | $w_-/w_+$ | Composition |
|---|---|---|---|---|---|---|---|
| Doublet 1 | 0.275 (55) | 0.75 (10) | 1730 (390) | 0.202 (72) | 1* | 1* | 7.0 (16) |
| | **CS (mm/s)** | **ε (mm/s)** | **A (counts.mm/s)** | **H(T) (mm/s)** | **$w_3$ (mm/s)** | | **Composition** |
| Sextet 1 | -0.040 (39) | 0.063 (39) | 1470 (570) | 33.16 (25) | 0.099 (52) | | 6.0 (23) |
| Sextet 2 | 0.1942 (55) | 0.0050 (54) | 21360 (720) | 20.796 (39) | 0.1655 (73) | | 87.0 (29) |
| **Reduced $\chi^2$ = 0.695895** | | | | | | | |

## SEM

The morphology of the samples was examined by SEM and is shown in Figures S3 and S4. $Ti_3C_2$-U10-Fe-800 displays interconnected flake-like particles, with small spherical particles dispersed on it. The absence of (002) peak in the PXRD can be explained by the fact that the flake-like MXene particles do not seem to have any particular arrangement. Flake-like particles are also present in the $Ti_3C_2$-U50-Fe-800 sample, with the figure showing more and smaller particles spread across the material. C-U50-Fe-800 (Figure S3C) shows the characteristic morphology of XC72R, and some CNTs with spherical particles encapsulated in them. In Figure S3D, the structure of a material that was synthesised following the same procedure as samples $Ti_3C_2$-U10-Fe-800 and $Ti_3C_2$-U50-Fe-800, but without any of the supports (XC72R or MXene). The material displays a porous network with bigger sphere-like particles attached to it, showing that the use of a support is helpful to avoid the coalescence of the Fe-containing species into bigger particles during thermal treatment.

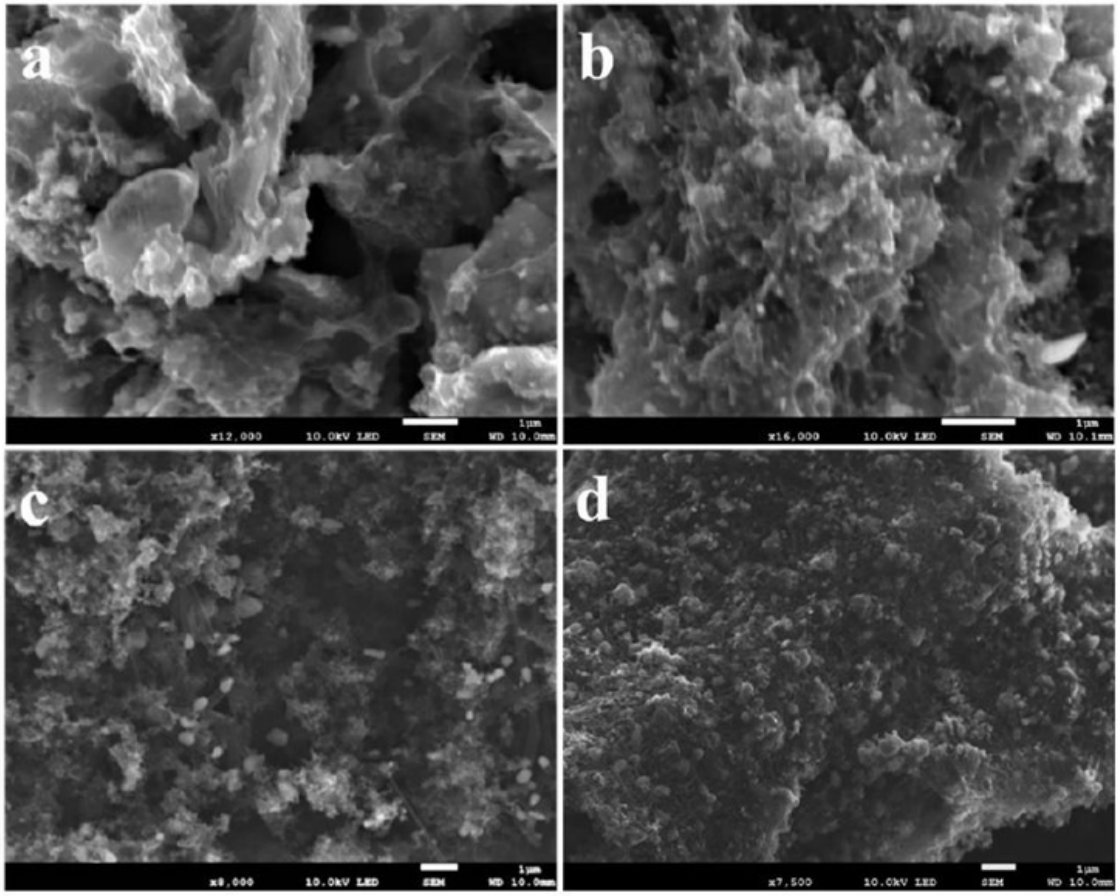


**Figure S3** SEM pictures of samples - a) $Ti_3C_2$-U10-Fe-800, b) $Ti_3C_2$-U50-Fe-800, c) C-U50-Fe-800 and d) U50-Fe-800 (scale bar is 1 μm).

Figure S4 shows that some differences between $Ti_3C_2$-U10-Fe-800 and $Ti_3C_2$-U50-Fe-800, as the latter seems to show formation of carbon nanotubes (CNTs) or carbon nanofibres (CNFs). As seen in the literature, Fe and/or $Fe_3C$ are both good catalysts for the growth of CNTs, and the Fe ions, after being reduced to $Fe_3C$ and Fe during the thermal treatment are allowing CNTs to grow on the carbon support through reaction with the products of decomposed urea. A higher amount of urea would allow for more decomposition products to

form and react with the Fe-species to form CNT/CNF on the sample, which would explain the higher amount seen in the sample with most urea. From Figures S3 and S4, it can be seen that introducing Fe precursors in either XC72R or MXene leads to the formation of carbon species on top of the supports. Comparable observations have been made in the literature, including Zhong et al [4] who made N-doped carbon nanotubes with encapsulated $Fe_3C$ and Fe by pyrolysis under Ar with a mix of melamine and $FeCl_3$ at 800 °C. It was shown that the Fe-precursor and the melamine mix would form $Fe_xO_y$ if pyrolysed at 650 °C but would undergo reduction to $Fe_3C$/Fe particles and encapsulate them.

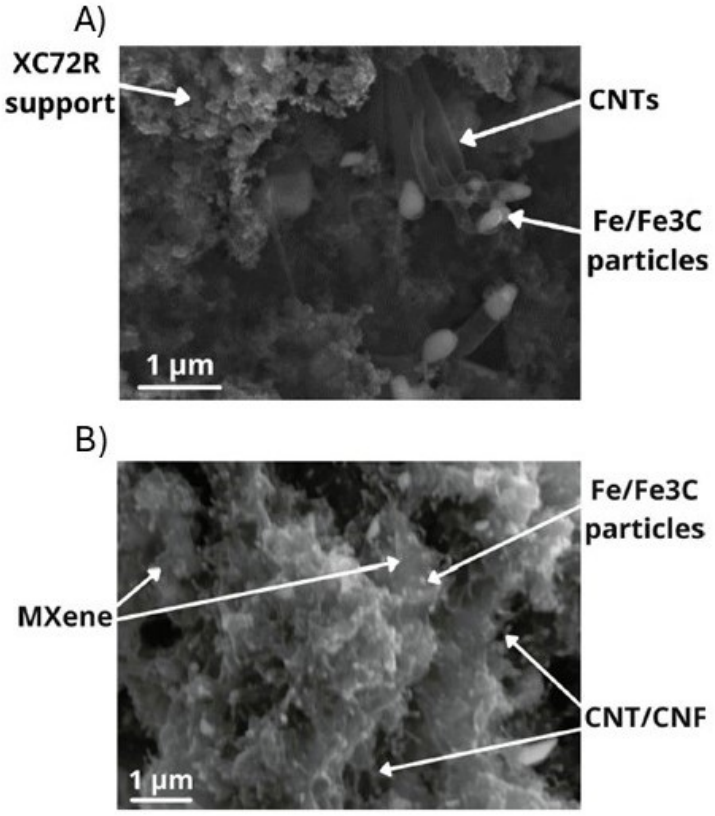


**Figure S4** SEM picture of samples with the different structures present. A) C-U50-Fe-800 and B) $Ti_3C_2$-U50-Fe-800.

## Nitrogen adsorption

To study the influence of the Fe precursors on the porosity and surface area of the samples, nitrogen adsorption and desorption experiments were carried out. Results are presented in Figure S5.

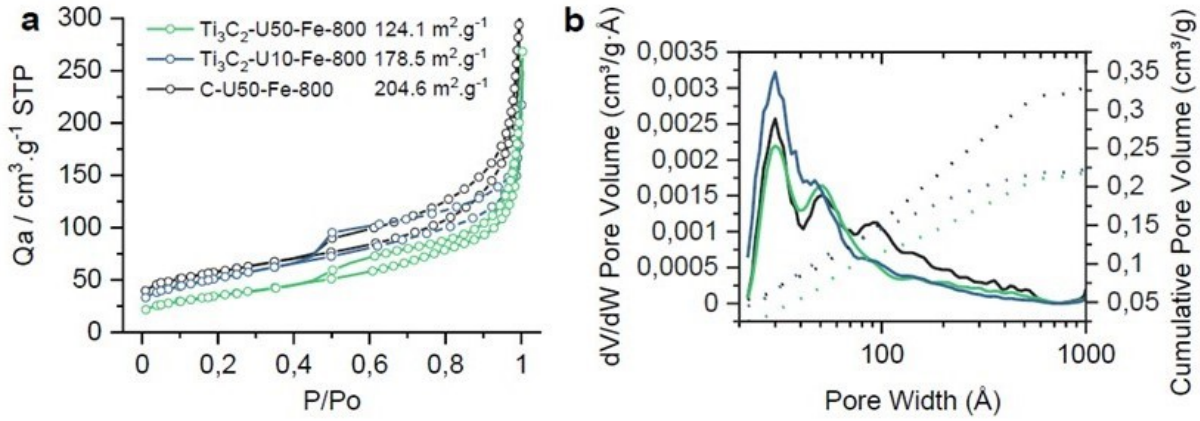


**Figure S5** Pore structure analysis of samples. a) Adsorption isotherms from $N_2$ adsorption-desorption experiments of $Ti_3C_2$-U10-Fe-800, $Ti_3C_2$-U50-Fe-800 and C-U50-Fe-800. The calculated surface area is given in the caption. b) Pore size distribution from NLDFT of the Fe-containing samples: cumulative pore volume (dotted line) and dV/dW pore volume (solid line).

As seen in Figure S5, the isotherms for all samples are type IV isotherms according to the IUPAC classification [5]. This is characteristic of porous materials that have mesopores (pore sizes ranging from 2 to 50 nm), which is due to the presence of the hysteresis loop representative of capillary condensation occurring in mesopores. For all samples, the hysteresis loop is a H3 hysteresis, which is the type seen for non-rigid aggregates of plate-like particles which display a slit-shaped pore. BET surface area measurements of the samples containing Fe show surface areas of 124.1 $m^2\ g^{-1}$ and 178.5 $m^2\ g^{-1}$ for the $Ti_3C_2$-U50-Fe-800 and $Ti_3C_2$-U10-Fe-800 respectively. The increase in surface area, along with the formation of carbonaceous species that contain nitrogen and $Fe_3C$ and Fe-$N_x$ should be beneficial for the electrochemical activity of the samples. The sample that used XC72R as a support (C-U50-Fe-800) shows a smaller BET surface area (204.6 $m^2\ g^{-1}$) than the stand-alone support XC72R (247.2 $m^2\ g^{-1}$). Figure S5 B shows the pore size distribution for the samples, determined using NLDFT with a slit pore model. Both $Ti_3C_2$-U10-Fe-800 and $Ti_3C_2$-U50-Fe-800 show cumulative pore volumes of 0.225 $cm^3\ g^{-1}$. Pore size distributions in both samples also show pore sizes centred around 3.0 nm and 4.9 nm and a broad pore size window from 10 to 60 nm. Pore size distribution is slightly different for the C-U50-Fe-800, with a cumulative pore volume of 0.3225 $cm^3\ g^{-1}$ and three distinct peaks at 3, 5 and 10 nm.

## XPS

Figure S6 shows the full X-ray Photoelectron Spectroscopy (XPS) spectra for the $Ti_3C_2$-U10-Fe-800, $Ti_3C_2$-U50-Fe-800, and C-U50-Fe-800, and the carbon to titanium and carbon to nitrogen ratio in the samples (with and without Fe).

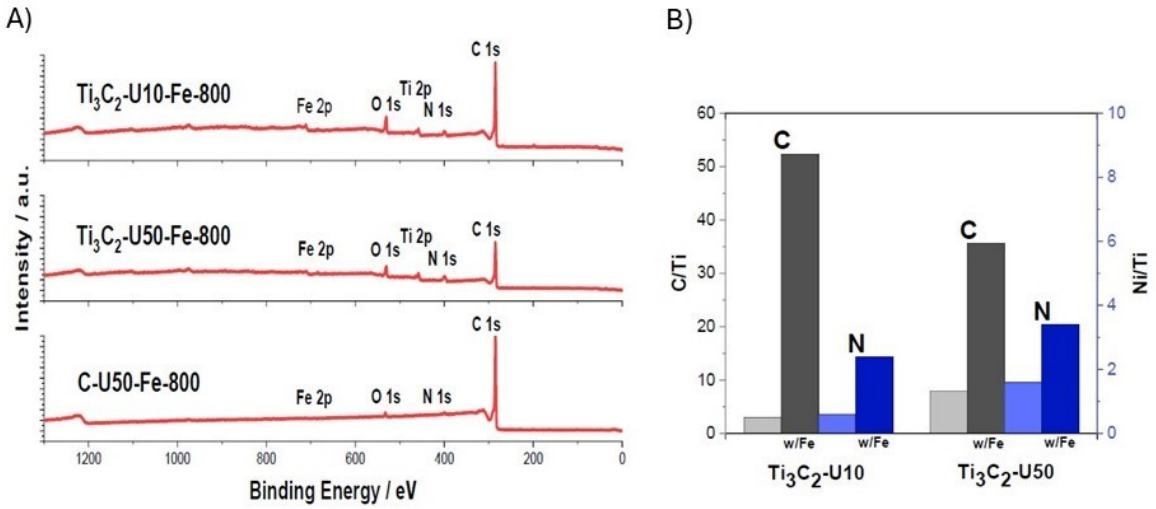


**Figure S6** XPS analysis of samples. A) Full XPS spectra of Fe-containing catalysts. B) Surface carbon and nitrogen content relative to Ti in samples treated at 800 °C with and without $Fe_3Cl$.

As can be observed in Figure S6, the main peak is around 282 – 292 eV, which corresponds to C 1s contribution, meaning that carbon is the biggest contributor to the surface chemistry of all samples. Figure S6 also shows the amount of surface carbon relative to Ti with and without Fe precursor, showing that samples with Fe precursor have a significantly higher amount of carbon on the surface. This is in accordance with results shown from XRD and SEM observations, meaning that it can be reasonably concluded that MXene flakes are covered with carbon species. In addition to the carbon peak, there are also peaks for Ti 2p, O 1s, N 1s, and Fe 2p. The small Fe 2p peak could be explained by the fact that Fe-species are encapsulated within carbon layers, which is what is usually reported when Fe species have been used as catalysts to grow carbon structures.

The peaks were further analysed to better understand the chemical structure of the surface. Tables S5 and S6 show the Ti 2p and N 1s peak fitting distribution for the samples.

**Table S5** Ti2p XPS peak fitting distribution.

| | **Ti-C $2p_{1/2}$ ($2p_{3/2}$)** | **$Ti^{2+}$ $2p_{1/2}$ ($2p_{3/2}$)** | **$Ti^{3+}$ $2p_{1/2}$ ($2p_{3/2}$)** | **$Ti^{4+}$ $2p_{1/2}$ ($2p_{3/2}$)** |
|---|---|---|---|---|
| **B.E. (eV) / (at %)** | 455.1 (460.4) | 456.2 (461.5) | 457.5 (462.8) | 458.8 (464.5) |
| $Ti_3C_2$-U10-Fe-800 | 4.09 | 24.37 | 27.03 | 44.83 |
| $Ti_3C_2$-U50-Fe-800 | 12.04 | 22.85 | 35.14 | 29.97 |

**Table S6** N1s XPS peak fitting distribution.

| | **N-Ti** | **N1** | **N2** | **N3** |
|---|---|---|---|---|
| **B.E. (eV) / (at %)** | 396.4 | 398.7 | 400.0 | 401.4 |
| $Ti_3C_2$-U10-Fe-800 | 19.78 | 43.31 | 12.55 | 24.37 |
| $Ti_3C_2$-U50-Fe-800 | 18.49 | 45.14 | 13.77 | 22.61 |

| | | | | |
|---|---|---|---|---|
| C-U50-Fe-800 | - | 39.21 | 37.45 | 23.34 |

The peak-fitting of X-ray Photoelectron Spectroscopy (XPS) spectra has been done using CasaXPS. The following constraints were applied during the peak-fitting of the samples, which were met for most of the components:

- A Gaussian-type distribution was chosen, assuming that deconvolution of the XPS spectra with Gaussian components would not greatly influence the analysis of the surface chemistry of the samples.
- Component and binding energy values were taken and based on studies focusing on the chemistry of MXenes, especially $Ti_3C_2$, carbides, nitrides, carbons, and N-doped carbons materials.
- The binding energy shift for a given component was constrained to a ± 0.5 eV window around the initial value.
- The full width at half maximum (FWHM) of a specific component was set, so that its value for a specific component would be similar in the different samples which would contain it.

In addition to these restrictions, another parameter specific to the Ti 2p spectra peak-fitting has been considered due to the $2p_{1/2}$ and $2p_{3/2}$ components:

- The peak splitting was kept within a window of 5 to 6 eV, as it includes the values which have generally been reported for the peak splitting between Ti $2p_{1/2}$ and Ti $2p_{3/2}$ for different Ti oxidation states. (ref 134)
- The intensity ratio between the Ti $2p_{1/2}$ and Ti $2p_{3/2}$ has been restricted according to:

$$I_{2p_{3/2}} = {}^{I_{2p_{1/2}}}\!/_{2}$$

Except for a few cases, the different constraints set for the deconvolution of the broad XPS peaks were met. The peak-fitting results for the different samples are given in tables S7, S8, and S9.

**Table S7** Ti2p XPS peak fitting parameters

| | **Ti-C** $2p_{1/2}$ / $2p_{3/2}$ | **$Ti^{2+}$** $2p_{1/2}$ / $2p_{3/2}$ | **$Ti^{3+}$** $2p_{1/2}$ / $2p_{3/2}$ | **$Ti^{4+}$** $2p_{1/2}$ / $2p_{3/2}$ |
|---|---|---|---|---|
| **$Ti_3C_2$-U10-Fe-800** | Residual: 0.894 | | | |
| Position (B.E. eV) | 455.20 / 460.01 | 456.20 / 461.00 | 457.66 / 462.77 | 458.70 / 464.37 |
| FWHM (eV) | 0.7 / 1.0 | 1.5 / 2.0 | 1.6 / 2.0 | 1.3 / 1.9 |
| **$Ti_3C_2$-U50-Fe-800** | Residual: 1.193 | | | |
| Position (B.E. eV) | 455.35 / 460.06 | 456.40 / 461.45 | 457.73 / 462.90 | 458.70 / 464.39 |
| FWHM (eV) | 1.1 / 2.0 | 1.3 / 1.9 | 1.7 / 2.0 | 1.2 / 1.5 |

**Table S8** C1s XPS peak fitting parameters

| | **C-Ti** | **C-Fe** | **C-C** | **C-O** | **N-C=N** | **C-F** | **π-π*** |
|---|---|---|---|---|---|---|---|
| **$Ti_3C_2$-U10-Fe-800** | Residual: 2.278 | | | | | | |
| Position (B.E. eV) | - | 283.87 | 284.81 | 285.80 | 287.86 | - | 290.47 |

| | | | | | | | |
|---|---|---|---|---|---|---|---|
| FWHM (eV) | - | 0.9 | 0.9 | 1.8 | 2.0 | - | 3.0 |
| **$Ti_3C_2$-U50-Fe-800** | Residual: 1.171 | | | | | | |
| Position (B.E. eV) | - | 283.90 | 284.77 | 285.80 | 287.85 | - | 290.27 |
| FWHM (eV) | - | 1.5 | 1.1 | 1.9 | 2.0 | - | 3.0 |
| **C-U50-Fe-800** | Residual: 3.155 | | | | | | |
| Position (B.E. eV) | - | 283.92 | 284.82 | 285.80 | 287.80 | - | 290.56 |
| FWHM (eV) | - | 0.9 | 0.9 | 1.9 | 2.0 | - | 3.0 |

**Table S9** N1s XPS peak fitting parameters

| | **N-Ti** | **N1 (pyridinic)** | **N2 (pyrrolic)** | **N3 (graphitic)** |
|---|---|---|---|---|
| **$Ti_3C_2$-U10-Fe-800** | Residual: 1.065 | | | |
| Position (B.E. eV) | 396.73 | 398.72 | 400.56 | 401.26 |
| FWHM (eV) | 1.5 | 1.9 | 2.0 | 1.9 |
| **$Ti_3C_2$-U50-Fe-800** | Residual: 0.981 | | | |
| Position (B.E. eV) | 396.54 | 398.57 | 400.54 | 401.14 |
| FWHM (eV) | 1.6 | 1.9 | 2.0 | 2.0 |
| **C-U50-Fe-800** | Residual: 0.844 | | | |
| Position (B.E. eV) | - | 398.80 | 400.49 | 401.67 |
| FWHM (eV) | - | 1.5 | 2.0 | 1.7 |

## References


1. Kramm, U.I., et al., *Correlations between Mass Activity and Physicochemical Properties of Fe/N/C Catalysts for the ORR in PEM Fuel Cell via 57Fe Mössbauer Spectroscopy and Other Techniques.* Journal of the American Chemical Society, 2014. **136**(3): p. 978-985.
2. Park, E., et al., *Characterization of phases formed in the iron carbide process by X-ray diffraction, mossbauer, X-ray photoelectron spectroscopy, and raman spectroscopy analyses.* Metallurgical and Materials Transactions B, 2001. **32**(5): p. 839-845.
3. Zhong, L., et al., *57Fe-Mössbauer spectroscopy and electrochemical activities of graphitic layer encapsulated iron electrocatalysts for the oxygen reduction reaction.* Applied Catalysis B: Environmental, 2018. **221**: p. 406-412.
4. Zhong, G., et al., *Nitrogen doped carbon nanotubes with encapsulated ferric carbide as excellent electrocatalyst for oxygen reduction reaction in acid and alkaline media.* Journal of Power Sources, 2015. **286**: p. 495-503.
5. Thommes, M., et al., *Physisorption of gases, with special reference to the evaluation of surface area and pore size distribution (IUPAC Technical Report).* Pure and Applied Chemistry, 2015. **87**(9-10): p. 1051-1069.